Research Article Vol. 56, No. 33 / November 20 2017 / Applied Optics 9341

applied optics

Phase retrieval in moiré volume computed tomography based on spatial phase shifting by triple-crossed gratings

Zhenyan Guo,[1] Qun Yuan,[1] Jia Wang,[2,*] Chao Zuo,[1,3] and Lei Chen[1]

[1]School of Electronic and Optical Engineering, Nanjing University of Science and Technology, Nanjing 210094, China
[2]School of Optical and Electronic Engineering, Xi'an Technological University, Xi'an 710021, China
[3]Jiangsu Key Laboratory of Spectral Imaging & Intelligence Sense, Nanjing University of Science and Technology, Nanjing 210094, China
*Corresponding author: wangjiar1001@126.com

Received 7 August 2017; revised 26 October 2017; accepted 27 October 2017; posted 27 October 2017 (Doc. ID 304357); published 20 November 2017

Due to its advantages of nonintrusiveness, wide measurement range, and insensitivity to variation, Moiré deflectometry is a powerful tool for quantitative measurement of a flow field's physical parameters such as density and temperature. Moiré volume computed tomography (MVCT), combining the moiré deflectometry and volume optical computed tomography (VOCT), can realize real three-dimensional parameters reconstruction, in which the radial derivatives extraction of the projected phase is of great importance. In this paper, a spatial phase-shifting-interferometry-based MVCT system was proposed to extract the radial shearing phase distribution. The system is simple and compact, and consists of three crossed gratings and lenses, with no wave plates or polarizers introduced. Via using a 4-f system, the optical path was shortened, and four spatial phase-shifting grid moiré projections can be obtained simultaneously. Each grid interferogram was filtered and separated into two linear interferograms in two orthogonal directions. Moreover, a two-step spatial phase-shifting algorithm was applied to obtain the first-order derivative phase in two mutually perpendicular directions, respectively. Simulations were implemented to verify the feasibility and accuracy of the proposed phase retrieval method. The measured results for the radial first-order partial derivative of the phase projection of a propane flame in the experimental VOCT system are presented.

OCIS codes: (110.6960) Tomography; (100.5070) Phase retrieval; (050.5080) Phase shift; (100.6950) Tomographic image processing.

https://doi.org/10.1364/AO.56.009341

1. INTRODUCTION

The measurements of transient three-dimensional (3D) physical parameters as density and temperature distribution of flow fields are of great importance for the flow field characteristics studies in aviation, aerospace, and energy engineering. Optical computerized tomography (OCT) is a combination of computerized tomography and optical technology, such as interferometery and moiré deflectometry. Owing to the advantages of being nonintrusive, instantaneous, and capable of 3D reconstruction, as well as having high temporal and spatial resolutions, OCT is an effective tool for various flow field diagnoses [1–5]. The moiré projection reflects the first partial derivatives of the phase, and therefore, by comparing with interference tomography, moiré tomography provides a wide measurement range but requires low mechanical stability. Therefore, moiré tomography has overwhelming superiorities in noisy environments for complex flow field diagnosis, such as a flame flow field [6], high-speed flow field [7], and supersonic wind tunnel [8] diagnoses.

Traditional moiré tomography reconstruction is a sophisticated stacking process [9,10]. Volume OCT (VOCT) based on 3D radon transform can be used to directly obtain the full-field spatial distribution and realize the real 3D full-field reconstruction, which is more effective in flow field diagnosis in the practical environment. In x-ray CT, the real 3D reconstruction can be realized via the VOCT method based on the cone-beam projection [11,12]. However, the projection of the 3D radon transform algorithm is produced on the condition of parallel-beam incidents. Transforming the parallel-beam projection applied in the cone-beam projection increases the computational complexity of the reconstruction process, and the larger cone angle of the cone-beam results in additional errors. In contrast, interferometry and moiré deflectometry tomography can be used to easily generate collimated-beam

incidence with a laser detection source. Therefore, the real 3D reconstruction can be rapidly and simply realized by the 3D radon transform based on the parallel-beam projection in OCT technology.

Acquiring the phase information from the moiré projections is critical in Moiré volume computed tomography (MVCT). The Fourier transform method has been used to extract the phase information from a single fringe projection acquired in VOCT [13]. Phase shifting is an accurate phase retrieval technology easily implemented in interferometry [14–16], in which the spatial phase shift works well in unstable environments by simultaneously capturing several phase-shifted interferograms. Spatial phase shift is usually realized by utilizing additional optical elements, such as polarizers and wave plates [17–19]. We have recently adopted spatial phase shifting in moiré tomography, and no polarizers or wave plates were introduced in the optical systems [20–22]. The spatial phase-shifting lateral shearing interferometry was demonstrated as a more suitable and effective technique for diagnosing transient flow fields. The elaborated intensity distribution expression of four interferograms, generated only by triple linear grating, were derived based on the scalar diffraction theory, and the phase shifting was found between the interferograms [20]. Moreover, the theoretical analysis and experimental verification of six-step spatial phase-shifting shearing interferometry was performed by crossed and linear gratings [21]. By using a 4-f system, the optical path is significantly shortened, and two complete spatial phase-shifting lateral shearing interferograms can be simultaneously obtained, resulting in a higher phase retrieve precision [22]. However, all of these proposed spatial phase-shifting techniques, to extract the phase information of moiré fringe, are applied to traditional moiré tomography.

In this paper, a new apparatus for the experimental system, including three crossed gratings, is presented to realize the spatial phase shift in MVCT. According to the 3D filtered back projection (FBP) algorithm, the transient physical parameters distribution as density and temperature of flow field can be reconstructed from the radial derivatives of the projected phase extracted in this work, which can be used for measuring and monitoring the combustion state in boilers, such as power plant boilers and steel-making boilers. In addition, the technology is also suitable for the cold flow field measurements, e.g., the hypersonic wind tunnel's density distribution measurements for flow field characteristics analyzing in aviation and aerospace engineering.

The phase projection was easily extracted by the spatial phase-shifted method. The details of the proposed optical path and spatial phase-shifted algorithm are provided in Section 2. The numerical simulation results of the phase projection retrieval are presented in Section 3. In Section 4, an experiment is performed to extract the radial first-order derivative of the phase information in the moiré fringes obtained by the optical configuration of MVCT. Section 5 provides a discussion regarding the present study and further applications of our proposed MVCT.

2. PRINCIPLES

A. Spatial Phase-Shifting Characteristics and Limitations of Shearing Interferometry by Double-Crossed Gratings

In order to realize the radial first-order derivative of the phase projection by spatial phase shifting in MVCT, considering the beam splitting and phase-shifting properties of gratings, the double-crossed gratings were placed instead of the linear gratings in the moiré optical configuration, and the setup is depicted in Fig. 1. Two crossed Ronchi gratings, G1 and G2, with the same grating constant d of 0.02 mm in both the horizontal and vertical directions were used to generate grid moiré fringes on the observation plane (OP). The two crossed gratings were oriented at angles $\alpha/2$ and $-\alpha/2$ relative to the y axis, respectively, as shown in Fig. 2. G1 and G2 were both placed parallel to the x–y plane and apart by a distance of Δ along the z axis.

Owing to the disturbance by the phase object, the optical field before G1 can be written as follows:

$$u_1^-(x,y) \propto \exp[ik\varphi(x,y)], \tag{1}$$

where $k = 2\pi/\lambda$, and λ is the wavelength of the incident light. $\varphi(x,y)$ is the phase projection of the distorted plane wave before G1. The transmittances of G1 and G2 can be described by the Fourier expansions:

$$g_1(x,y) = \sum_{n_1} a_{n_1} \exp\left[\frac{i2\pi n_1}{d}\left(x\cos\frac{\alpha}{2} - y\sin\frac{\alpha}{2}\right)\right] \times \sum a_{m_1} \exp\left[\frac{i2\pi m_1}{d}\left(x\sin\frac{\alpha}{2} + y\cos\frac{\alpha}{2}\right)\right], \tag{2}$$

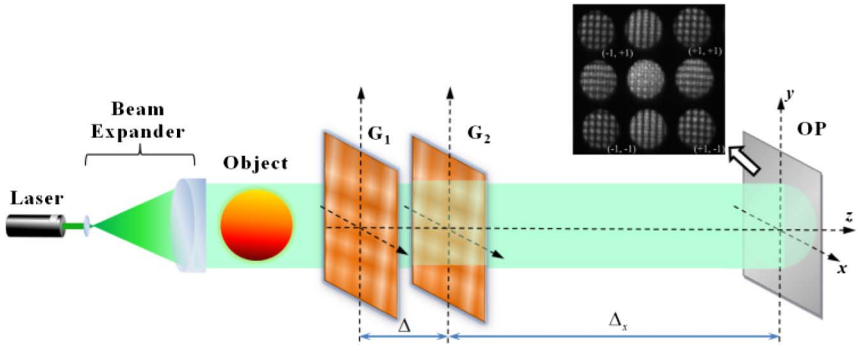

Fig. 1. Optical configuration of double-crossed gratings interferometry.

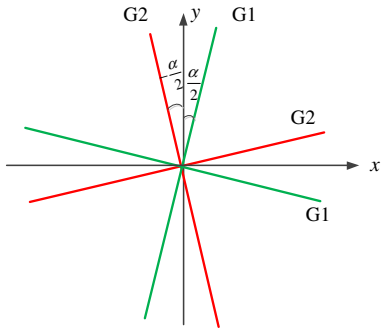

Fig. 2. Locations and orientations of two crossed gratings.

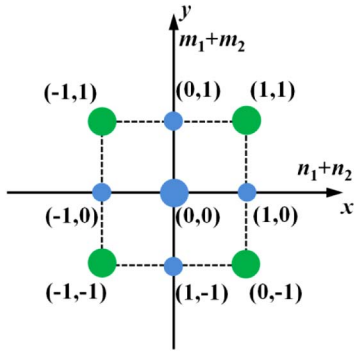

Fig. 3. Frequency spectrum distribution of the interferograms.

$$g_2(x,y)=\sum_{n_2}a_{n_2}\exp\left[\frac{i2\pi n_2}{d}\left(x\cos\frac{\alpha}{2}+y\sin\frac{\alpha}{2}\right)\right]\times\sum_{m_2}a_{m_2}\exp\left[\frac{i2\pi m_2}{d}\left(-x\sin\frac{\alpha}{2}+y\cos\frac{\alpha}{2}\right)\right],\tag{3}$$

where a_{n_1}, a_{m_1}, a_{n_2}, and a_{m_2} are the Fourier expansion coefficients in two orthogonal directions. Applying the complex amplitude calculation method based on the scalar diffraction theory [21], the field $u_3^-(x,y)$ before the OP is described as

$$\begin{aligned}u_3^-(x,y)&=\sum_{n_1}a_{n_1}\sum_{m_1}a_{m_1}\sum_{n_2}a_{n_2}\sum_{m_2}a_{m_2}\exp\{ik(\Delta+\Delta_x)\}\\&\times\exp\left\{-\frac{i\pi\Delta\lambda}{d^2}\left(n_1^2\cos\frac{\alpha}{2}+m_1^2\right)\right\}\\&\times\exp\left\{\frac{i2\pi}{d}\left(n_1\cos\frac{\alpha}{2}+m_1\sin\frac{\alpha}{2}+n_2\cos\frac{\alpha}{2}-m_2\sin\frac{\alpha}{2}\right)x\right\}\\&\times\exp\left\{\frac{i2\pi}{d}\left(-n_1\sin\frac{\alpha}{2}+m_1\cos\frac{\alpha}{2}+n_2\sin\frac{\alpha}{2}+m_2\cos\frac{\alpha}{2}\right)y\right\}\\&\times\exp\left\{\frac{-i\pi\Delta_x\lambda}{d^2}\begin{bmatrix}n_1^2+n_1^2+n_1^2+n_1^2+2(n_1n_2+m_1m_2)\cos\alpha\\+2(n_2m_1-n_1m_2)\sin\alpha\end{bmatrix}\right\}\\&\times\exp\{ik\varphi(x,y)\}\\&\times\exp\left\{-ik\frac{\partial\varphi(x,y)}{\partial x}C_x\right\}\exp\left\{-ik\frac{\partial\varphi(x,y)}{\partial y}C_y\right\},\end{aligned}\tag{4}$$

where

$$C_x=\frac{\lambda}{d}\begin{bmatrix}\left(n_1\cos\frac{\alpha}{2}+m_1\sin\frac{\alpha}{2}\right)\Delta\\+\left((n_1+n_2)\cos\frac{\alpha}{2}+(m_1-m_2)\sin\frac{\alpha}{2}\right)\Delta_x\end{bmatrix},\tag{5}$$

$$C_y=-\frac{\lambda}{d}\begin{bmatrix}\left(n_1\cos\frac{\alpha}{2}+m_1\sin\frac{\alpha}{2}\right)\Delta\\+\left((n_1-n_2)\cos\frac{\alpha}{2}-(m_1+m_2)\sin\frac{\alpha}{2}\right)\Delta_x\end{bmatrix}.\tag{6}$$

In Eq. (4), the complex amplitude distribution $u_3^-(x,y)$ of the optical field contains several diffraction orders. Given that the diffractive energy is almost focused on the diffraction orders of −1, 0, and +1, the frequency spectra distributions of the optical field that satisfy the equations $m_1+m_2=(-1,0,1)$ and $n_1+n_2=(-1,0,1)$ are illustrated in Fig. 3. If the distance of Δ_x between G2 and OP is too large, the moiré fringes corresponding to all of the orders of frequency spectra will project on the OP [21]. By substituting the diffraction orders of each interferogram into Eq. (4), we can obtain the intensity distribution of each interferogram. The accurate spatial phase shifts can be found between the interferograms with diffraction orders (1, 1), (1, −1), (−1, 1), and (−1, −1), as described by Eq. (7):

$$\begin{cases}I_{1,1}(x,y)=4a_0^4a_1^4[1+\cos(\Phi_x-\mathrm{ps}_1-\mathrm{ps}_2)]\times[1+\cos(\Phi_y+\mathrm{ps}_1-\mathrm{ps}_2)]\\I_{1,-1}(x,y)=4a_0^4a_1^4[1+\cos(\Phi_x+\mathrm{ps}_1-\mathrm{ps}_2)]\times[1+\cos(\Phi_y+\mathrm{ps}_1+\mathrm{ps}_2)]\\I_{-1,1}(x,y)=4a_0^4a_1^4[1+\cos(\Phi_x-\mathrm{ps}_1+\mathrm{ps}_2)]\times[1+\cos(\Phi_y-\mathrm{ps}_1-\mathrm{ps}_2)]\\I_{-1,-1}(x,y)=4a_0^4a_1^4[1+\cos(\Phi_x+\mathrm{ps}_1+\mathrm{ps}_2)]\times[1+\cos(\Phi_y-\mathrm{ps}_1+\mathrm{ps}_2)]\end{cases},\tag{7}$$

where

$$\begin{cases}\Phi_x=\begin{bmatrix}\frac{4\pi}{d}x\sin\frac{\alpha}{2}-\frac{2\pi\Delta}{d}\frac{\partial\varphi(x,y)}{\partial y}\cos\frac{\alpha}{2}\\-\frac{2\pi(\Delta+2\Delta_x)}{d}\frac{\partial\varphi(x,y)}{\partial x}\sin\frac{\alpha}{2}\end{bmatrix}\\\Phi_y=\begin{bmatrix}\frac{4\pi}{d}y\sin\frac{\alpha}{2}+\frac{2\pi\Delta}{d}\frac{\partial\varphi(x,y)}{\partial x}\cos\frac{\alpha}{2}\\-\frac{2\pi(\Delta+2\Delta_x)}{d}\frac{\partial\varphi(x,y)}{\partial y}\sin\frac{\alpha}{2}\end{bmatrix}\\\mathrm{ps}_1=\frac{\pi\Delta\lambda}{d^2}\\\mathrm{ps}_2=\frac{2\pi\Delta_x\lambda}{d^2}\sin\alpha\end{cases}.\tag{8}$$

From Eq. (7), the intensity of each interferogram has a strict cosinusoidal distribution in both the x and y directions. Meanwhile, the obvious phase shifts generated by the distance of Δ and Δ_x exist between the first-order interferograms $I_{1,1}$, $I_{1,-1}$, $I_{-1,1}$, and $I_{-1,-1}$ in both the horizontal and vertical directions. In the moiré volume tomography scheme depicted in Fig. 1, four spatial phase-shifted interferograms can be acquired simultaneously, as well as the simultaneous phase shift in two orthogonal directions. Therefore, by combining the theoretical derivations, the spatial phase-shift method may be used to

retrieve the partial derivative phase information of the test flow field in orthogonal directions using the optical configuration shown in Fig. 1.

The splitting characteristics of the gratings was utilized to realize the synchronization acquisition of several phase-shifted interferograms in the optical path shown in Fig. 1. Owing to the low diffraction efficiency of the gratings, the optical path was long enough to separate the spatial phase-shifted interferograms from each other. Using the following experimental parameters, a grating period of 0.02 mm, detection wavelength of 532.8 nm, and a light aperture of 50 mm the distance Δ_x was calculated as 2 m. Therefore, the optical system was too long to apply in practice. Furthermore, Eq. (8) provides only an approximate value and is based on the assumption that the distance Δ_x has an infinitesimal value. When the value of Δ_x is large, the partial derivative in the x direction $(\partial\varphi(x,y)/\partial x)(\Delta + 2\Delta_x)\sin(\alpha/2)$ in phase Φ_x and in the y direction $(\partial\varphi(x,y)/\partial y)(\Delta + 2\Delta_x)\sin(\alpha/2)$ in phase Φ_y cannot be omitted, but was omitted in the practical phase retrieval. Moreover, the higher-order partial derivatives, such as $\partial^2\varphi(x,y)/\partial x$, $\partial^2\varphi(x,y)/\partial y$, and $\partial^2\varphi(x,y)/\partial x\partial y$ modulated by Δ_x, omitted in phase shifting ps_1 and ps_2, should be listed in Eq. (8). Therefore, Eq. (8) becomes too complex to extract the phase information from the phase-shifted interferograms.

B. Optical Configuration of Spatial Phase-Shifted Moiré Volume Tomography System Based on Triple-Crossed Gratings

To overcome the disadvantages of the double-crossed grating configuration shown in Fig. 1, a 4-f system was introduced and located behind the double-crossed gratings, which is shown in Fig. 4. In this new optical configuration, not only the value of Δ_x is zero, but also the optical path is significantly shortened to 1.2 m, which is directly calculated by the 0.4 m focal length of the lens in 4-f system.

By considering the small refractive index variation of the test propane flame in the cross-section along the x direction, the double-crossed gratings were rotated at an angle of θ in the x–y plane, with a small angle α between each. For simplicity, a new coordinate system $x' - y'$ was defined through the rotation of the x–y coordinate system with an angle of θ around the z axis. The x'–y' coordinate system is described by $x' = x\cos\theta + y\sin\theta$ and $y' = -x\sin\theta + y\cos\theta$, based on the coordinate system transformation shown in Fig. 5.

As shown in Fig. 4, another crossed grating G3 and two filters (F1 and F2) were inserted in the 4-f system to simultaneously capture the four first-diffracted-order spatial phase-shifted interferograms in one frame. The filter F1 was placed in front of the spectral plane of the $4 - f$ system to filter out the interferograms of diffraction order (1, 1), (1, −1), (−1, 1), and (−1, −1). The crossed grating G3 was set on the spectrum plane of the 4-f system to duplicate the four first-diffracted-order interferograms. After the spectrum plane, the filter F2 was located to filter out the (1, 1), (1, −1), (−1, 1), and (−1, −1) diffraction order interferograms simultaneously on the OP. The structure details of F1 and F2 are illustrated in Fig. 4, and the red circled areas are transparent.

In this triple-crossed gratings optical configuration, the distance Δ_x is zero, so the intensity distribution of the four first-order interferograms in Eqs. (7) and (8) can be written as

$$\begin{cases} I_{1,1}(x',y') = 4a_0^4a_1^4\left[1+\cos\left(\Phi_x - \frac{\pi\Delta\lambda}{d^2}\right)\right]\left[1+\cos\left(\Phi_y + \frac{\pi\Delta\lambda}{d^2}\right)\right] \\ I_{1,-1}(x',y') = 4a_0^4a_1^4\left[1+\cos\left(\Phi_x + \frac{\pi\Delta\lambda}{d^2}\right)\right]\left[1+\cos\left(\Phi_y + \frac{\pi\Delta\lambda}{d^2}\right)\right] \\ I_{-1,1}(x',y') = 4a_0^4a_1^4\left[1+\cos\left(\Phi_x - \frac{\pi\Delta\lambda}{d^2}\right)\right]\left[1+\cos\left(\Phi_y - \frac{\pi\Delta\lambda}{d^2}\right)\right] \\ I_{-1,-1}(x',y') = 4a_0^4a_1^4\left[1+\cos\left(\Phi_x + \frac{\pi\Delta\lambda}{d^2}\right)\right]\left[1+\cos\left(\Phi_y - \frac{\pi\Delta\lambda}{d^2}\right)\right] \end{cases}, \tag{9}$$

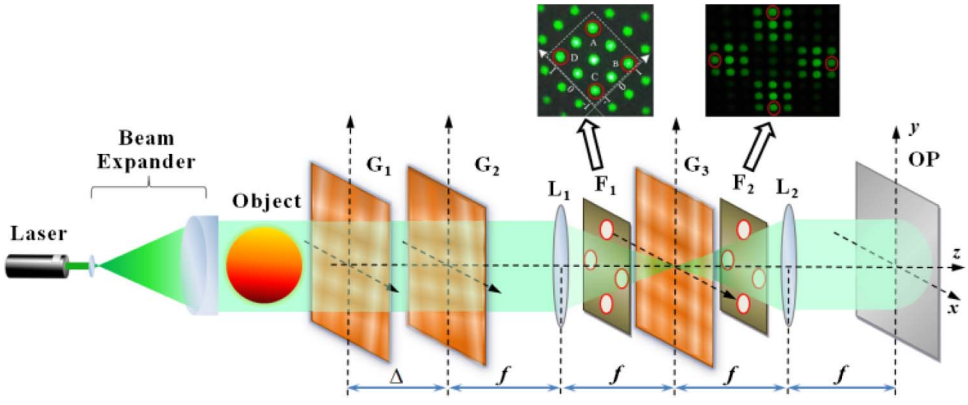

Fig. 4. Optical configuration of moiré volume tomography based on triple-crossed gratings.

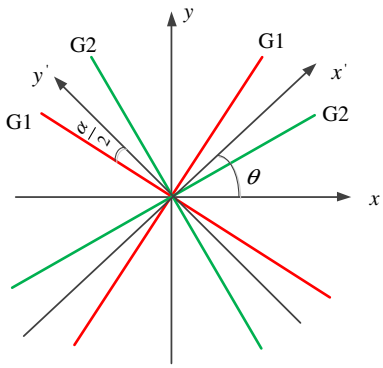

Fig. 5. Rotated coordinate system $x' - y'$ and locations of the two rotated crossed gratings.

where

$$\begin{cases} \Phi_x = \frac{4\pi}{d}x' \sin\frac{\alpha}{2} - \frac{2\pi\Delta}{d}\frac{\partial\varphi(x',y')}{\partial y'} \cos\frac{\alpha}{2} - \frac{2\pi\Delta}{d}\frac{\partial\varphi(x',y')}{\partial x'} \sin\frac{\alpha}{2} \\ \Phi_y = \frac{4\pi}{d}y' \sin\frac{\alpha}{2} + \frac{2\pi\Delta}{d}\frac{\partial\varphi(x',y')}{\partial x'} \cos\frac{\alpha}{2} - \frac{2\pi\Delta}{d}\frac{\partial\varphi(x',y')}{\partial y'} \sin\frac{\alpha}{2} \end{cases}. \tag{10}$$

The term $\pi\Delta\lambda/d^2$ indicates the spatial phase-shifted amount that exists in the four first-diffracted-order interferograms in both the x' and y' directions simultaneously. So the phase-shifted amount directly depends on the distance Δ between the double-crossed gratings G1 and G2.

C. Spatial Phase-Shift Algorithm

For simplicity, Eq. (9) can be rewritten as

$$\begin{cases} I_{1,1}(x',y') = 2a_0^2a_1^2[1+\cos(\Phi_x - \xi)] \times 2a_0^2a_1^2[1+\cos(\Phi_y + \xi)] \\ I_{1,-1}(x',y') = 2a_0^2a_1^2[1+\cos(\Phi_x + \xi)] \times 2a_0^2a_1^2[1+\cos(\Phi_y + \xi)] \\ I_{-1,1}(x',y') = 2a_0^2a_1^2[1+\cos(\Phi_x - \xi)] \times 2a_0^2a_1^2[1+\cos(\Phi_y - \xi)] \\ I_{-1,-1}(x',y') = 2a_0^2a_1^2[1+\cos(\Phi_x + \xi)] \times 2a_0^2a_1^2[1+\cos(\Phi_y - \xi)] \end{cases}, \tag{11}$$

where $\xi = \pi\lambda\Delta/d^2$. In consideration of the small value of Δ and minimal value of α, Eq. (10) can be simplified as

$$\begin{cases} \Phi_x = \frac{4\pi}{d}x' \sin\frac{\alpha}{2} - \frac{2\pi\Delta}{d}\frac{\partial\varphi(x',y')}{\partial y'} \cos\frac{\alpha}{2} \\ \Phi_y = \frac{4\pi}{d}y' \sin\frac{\alpha}{2} + \frac{2\pi\Delta}{d}\frac{\partial\varphi(x',y')}{\partial x'} \cos\frac{\alpha}{2} \end{cases}. \tag{12}$$

In order to separate the first-order partial derivative of the phase projection in the x' and y' directions, the $(1,-1)$ and $(-1,1)$ diffraction order moiré fringes were chosen and processed in the frequency domain in which the phase shifting existed in both the x' and y' directions simultaneously.

First, a 2D Fourier transform was applied in the $(1,-1)$ and $(-1,1)$ diffraction order interferograms to filter out the intensity distribution of the phase projections in the x' and y' directions, respectively, which can be written as

$$\begin{cases} I_1^x = 2a_0^2a_1^2 \cos(\Phi_x + \xi) \\ I_2^x = 2a_0^2a_1^2 \cos(\Phi_x - \xi) \end{cases}, \tag{13}$$

$$\begin{cases} I_1^y = 2a_0^2a_1^2 \cos(\Phi_y + \xi) \\ I_2^y = 2a_0^2a_1^2 \cos(\Phi_y - \xi) \end{cases}, \tag{14}$$

where I_1^x and I_2^x are the intensity distributions of the $(1,-1)$ and $(-1,1)$ diffraction order interferograms for the x' direction phase information, respectively, and I_1^y and I_2^y are the corresponding intensity distributions for the y' direction. Phase shifting clearly occurs in both I_1^x and I_2^x, and I_1^y and I_2^y.

The two-step phase shifting method can be used to extract the phase information Φ_x and Φ_y. If the distance between the double-crossed gratings is not a sub-Talbot distance, i.e., the phase shift ξ satisfies $\xi \neq (k\pi \pm \pi/2)$, the two-step phase-shifting algorithm can be easily derived from Eqs. (13) or (14), e.g., for phase retrieval in the x' direction:

$$\Phi_x = \arctan\left[\left(\frac{I_1^x - I_2^x}{I_1^x + I_2^x}\right)\cot\xi\right]. \tag{15}$$

In order to remove the tilting term of the phase Φ_x^r $[\Phi_x^r = (4\pi/d)x' \sin(\alpha/2)]$ from Φ_x, the phase projection of the reference interferograms should be measured. The reference moiré fringes can be obtained when no phase object is placed in the optical configuration.

Then, the first-order partial derivative of the phase information in the y' direction can be written as

$$\frac{\partial\varphi(x',y')}{\partial y'} = \frac{\Phi_x - \Phi_x^r}{2\pi\Delta \cos(\alpha/2)/d}. \tag{16}$$

With the same method, the first-order partial derivative of the phase information in x' direction is

$$\frac{\partial\varphi(x',y')}{\partial x'} = \frac{\Phi_y - \Phi_y^r}{2\pi\Delta \cos(\alpha/2)/d}. \tag{17}$$

Finally, the radial first-order partial derivative of the phase information can be derived as

$$\frac{\partial\varphi(r)}{\partial r} = \frac{\partial\varphi(x',y')}{\partial x'}\cos\varphi + \frac{\partial\varphi(x',y')}{\partial y'}\sin\varphi. \tag{18}$$

3. NUMERICAL SIMULATION

A numerical simulation experiment was performed to verify the spatial phase-shift algorithm with the following parameters: $\lambda = 532.8$ nm, $d = 0.02$ mm, $\alpha = 0.001$ rad, and Δ 10 mm, with 128×128 pixels contained in each moiré pattern.

A. Phase Retrieval of Reference Interferograms when No Phase Object Exists

Using Eq. (11), for no phase object in the optical configuration, the intensity distribution of the $(1,-1)$ and $(-1,1)$ diffraction orders grid interferograms were calculated and are shown in Figs. 6(a) and 6(b).

Applying the frequency domain processing method described in Section 2.C, the reference interferograms of the $(1,-1)$ and $(-1,1)$ diffraction orders, including only the x or y direction phase information, are shown in Figs. 6(c)–6(f). Furthermore, the reference phase information Φ_x^r and Φ_y^r were extracted by the two-step phase-shifting method described by Eq. (15), and the results are shown in Figs. 6(g) and 6(h).

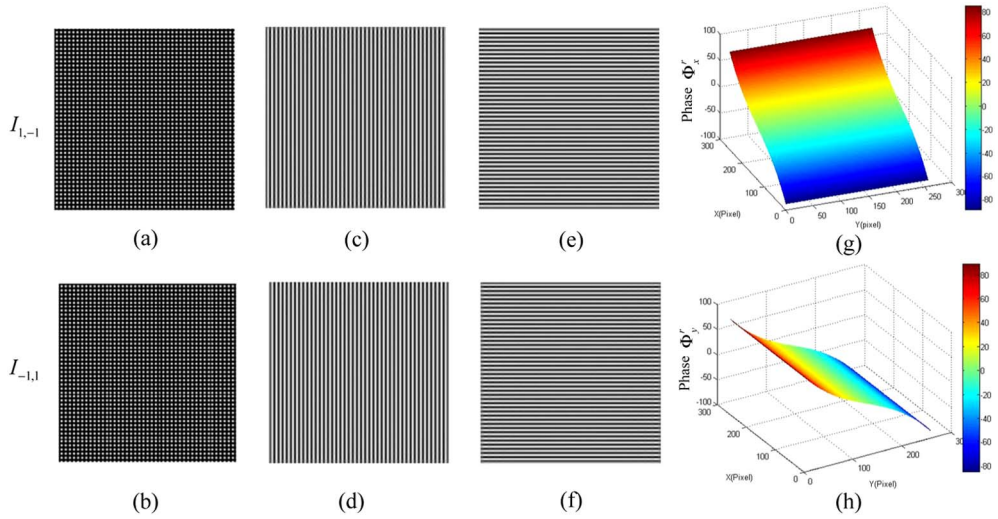

Fig. 6. Phase distribution of reference moiré fringe in the x and y directions: (a) reference grid moiré fringe of the $(1, -1)$ diffraction orders, (b) reference grid moiré fringe of the $(-1, 1)$ diffraction orders, (c) reference moiré fringe I_1^x, (d) reference moiré fringe I_2^x, (e) reference moiré fringe I_1^y, (f) reference moiré fringe I_2^y, (g) phase distribution in the x direction Φ_x^r, and (h) phase distribution in the y direction Φ_y^r.

B. Phase Retrieval of Interferograms when a Phase Object Exists

A Gaussian function was used to simulate the phase projection distribution, defined as

$$\varphi(x, y) = \frac{\sqrt{2\pi}}{12500} \exp\left(\frac{x^2 + y^2}{-0.0001}\right). \tag{19}$$

The phase projection area was 50 mm × 50 mm and was evenly sampled with 512 × 512 pixels. Using Eq. (19), the first-order partial derivatives of the phase information in the x, y, and r directions were calculated and are shown in Fig. 7.

Furthermore, the intensity distribution of the $(1, -1)$ and $(-1, 1)$ diffraction orders deflected grid interferograms $I_{(1,-1)}$ and $I_{(-1,1)}$ are shown in Figs. 8(a) and 8(b), respectively. The moiré patterns in the x and y directions were separated in the frequency domain as indicated in Figs. 8(c)–8(f). The phase information Φ_x and Φ_y were then retrieved by the two-step phase-shifting method shown in Figs. 8(g) and 8(h), respectively. By removing the tilting term of the phase Φ_x^r in the reference fringes shown in Fig. 8, the first-order partial derivatives in the x and y directions of the Gaussian phase projection were obtained by Eqs. (16) and (17) and are plotted in Figs. 9(a) and 9(b). Figure 9(c) shows the final radial partial derivative of the Gaussian phase projection calculated by Eq. (18).

By comparing Figs. 7(c) and 9(c), the phase retrieval results were consistent with the derived phase distribution displayed in Fig. 10. This showed that the proposed spatial phase-shifting method can be used to measure the radial first-order partial derivative of a tested wavefront with high accuracy.

4. EXPERIMENT

An experimental system was built according to the optical layout shown in Fig. 4 to test the flow field of the propane flame. The basic parameters were the same as in the simulated experiment described in Section 3. In particular, the distance between the double-crossed gratings G1 and G2 was 10 mm, which indicated that the phase shift ξ was $3\pi/10$. The angle α between the double-crossed gratings was ~0.0041 rad, which was calculated according to the fringe width in the interferograms. A CCD was located in front of the OP to capture the interferograms $I_{(1,-1)}$ and $I_{(-1,1)}$, with a resolution of 2448 × 2050 (Allied Vision technologies GC2450). The original reference and deflection grid interferograms $I_{(1,-1)}$ and $I_{(-1,1)}$, were acquired in the first and second shots with the frame rate of 15 fps, and are shown

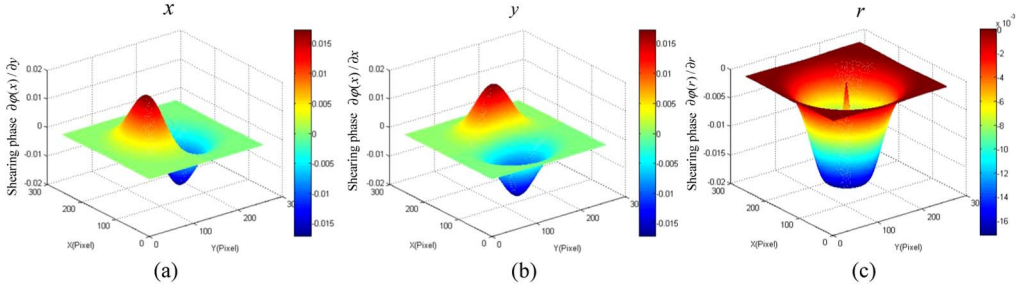

Fig. 7. Derived first-order partial derivative of the phase distribution: (a) $\partial\varphi(x)/\partial x$ in the x direction, (b) $\partial\varphi(y)/\partial y$ in the y direction, and (c) $\partial\varphi(r)/\partial r$ in the r direction.

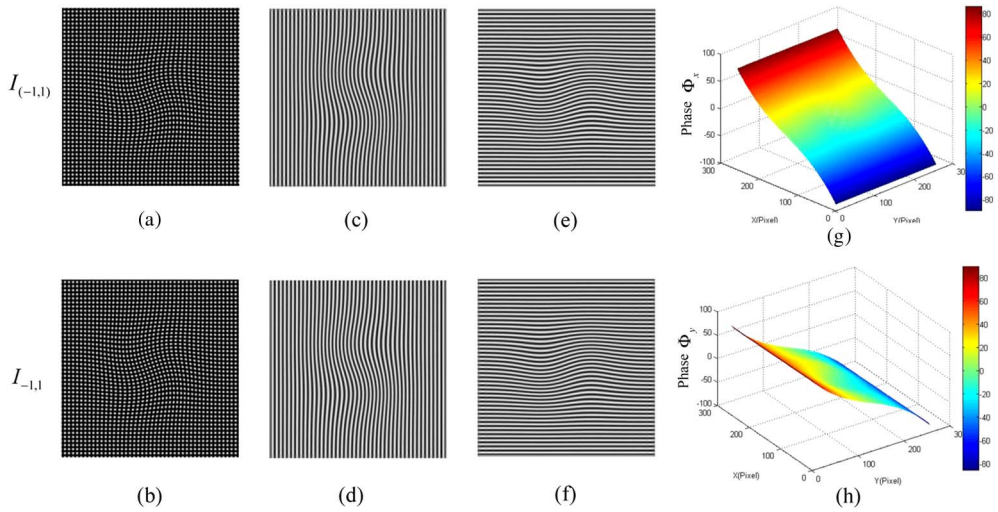

Fig. 8. Phase distribution of the moiré patterns with Gaussian phase projections in the x and y directions: (a) grid moiré pattern of the (1, −1) diffraction orders, (b) grid moiré fringe of the (−1, 1) diffraction orders, (c) moiré fringe I_1^x, (d) moiré fringe I_2^x, (e) moiré fringe I_1^y, (f) moiré fringe I_2^y, (g) phase distribution in x direction Φ_x, and (h) phase distribution in the y direction Φ_y.

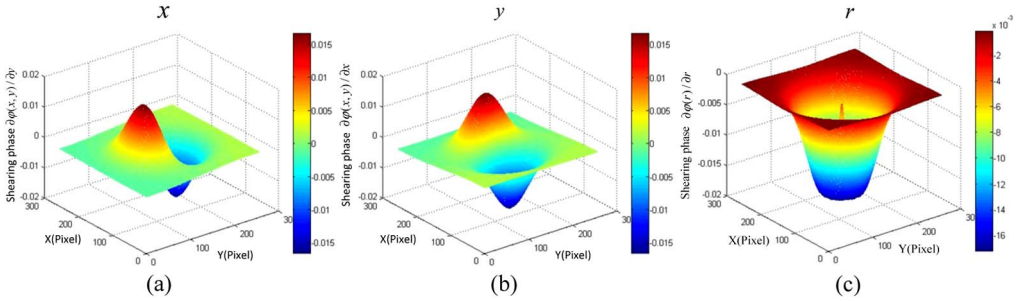

Fig. 9. Retrieval of the first-order partial derivative of Gaussian phase projections: (a) $\partial\varphi(y)/\partial y$ in the x direction, (b) $\partial\varphi(x)/\partial x$ in the y direction, and (c) $\partial\varphi(r)/\partial r$ in the r direction.

in Figs. 11(a) and 11(b), respectively. The radial partial derivative phase extracted off-line with MATLAB 2014 in total consumed 10 s using a PC (Intel Core i5 CPU, 8G memory size, win7 64-bit system, 250G hard disk).

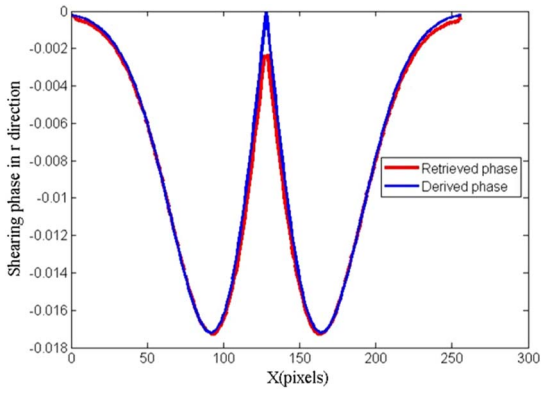

Fig. 10. Comparison between retrieved and derived phase results in a line.

After the calibration of the interferograms $I_{(1,-1)}$ and $I_{(-1,1)}$, the two grid moiré images were well matched point to point. The calibrated interferograms are displayed in Figs. 11(c)–11(f), and the red square area was chosen for the processing.

Figures 12(a) and 12(b) show the separated deflected moiré fringes $I_{(1,-1)}$ and $I_{(-1,1)}$ in the x' and y' directions using the frequency domain processing method, and Figs. 12(c) and 12(d) show the separated results of the reference moiré fringes. The extracted phase information without a phase object and with the propane flame in the double orthogonal direction is shown in Figs. 13(a) and 13(b), respectively. Furthermore, by removing the tilting terms of the shearing phase Φ^r from the shearing phase Φ, the first-order partial derivatives in the x' and y' directions of the propane flame phase distribution are displayed in Fig. 13(c). Figure 14 shows the final first-order partial derivative in the r direction of the propane flame. The temperature in the center of the flame is lower than at the edge [13]. Furthermore, Fig. 14 indicates that the test flame is just an approximate axisymmetric flow field. In order to reconstruct the real temperature distribution more precisely, multidirectional phase projections should be acquired according to

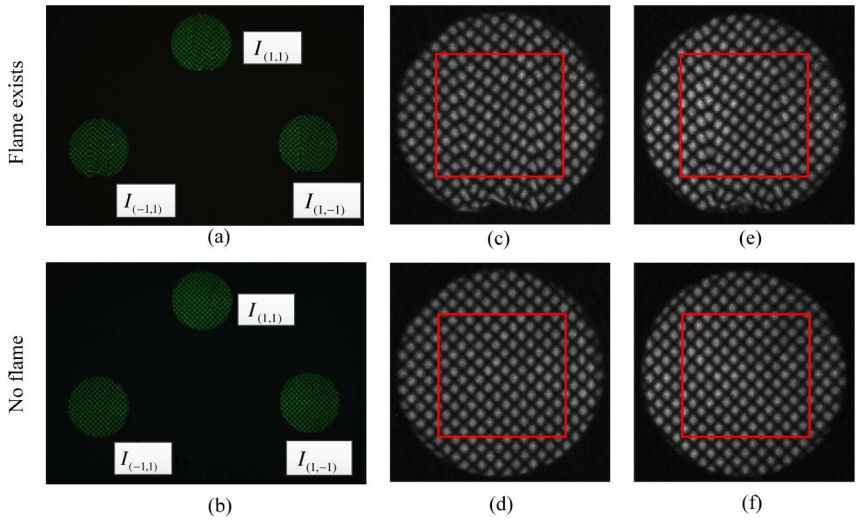

Fig. 11. Original grid interferograms: (a) reference interferograms captured by the CCD, (b) deflected interferograms captured by the CCD with a propane flame, (c) deflected interferograms $I_{(1,-1)}$ after calibration, (d) reference interferograms $I_{(1,-1)}$ after calibration, (e) deflected interferograms $I_{(-1,1)}$ after calibration, and (f) reference interferograms $I_{(-1,1)}$ after calibration.

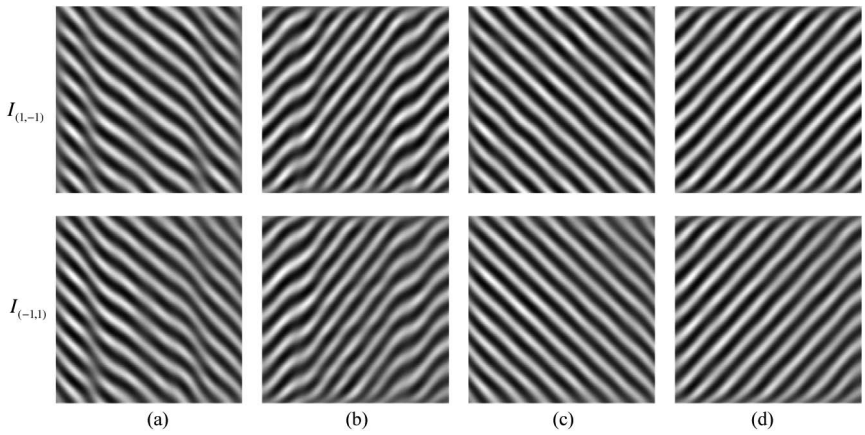

Fig. 12. Separated interferograms in the orthogonal direction: (a) deflected moiré patterns in the x direction, (b) deflected moiré patterns in the y direction, (c) reference moiré patterns in the x direction, and (d) deflected moiré patterns in the y direction.

the FBP algorithm [5]. Thus, in our further work, the multidirectional spatial phase-shifting MVCT system should be established based on the single directional spatial phase-shifting MVCT configuration proposed in this paper.

5. CONCLUSION

In this paper, a simple optical path consisting of triple-crossed gratings was presented to realize phase retrieval with a spatial phase-shifting method in MVCT. The phase shifting in the double orthogonal direction was simultaneously generated between the grid interferograms with (1, 1), (1, −1), (−1, 1), and (−1, −1) diffraction orders using double-crossed gratings located just behind the test flow field. The four first-order grid interferograms were duplicated by a third crossed grating placed on the frequency spectrum plane of a 4-f system, and two simple filters were inserted in the 4-f system to sufficiently filter out the four spatial phase-shifting interferograms. Four desired spatial phase-shifting grid interferograms were then simultaneously acquired with high clarity on the OP in a compact optical configuration.

The grid interferograms of the (1, −1) and (−1, 1) diffraction orders with simultaneous phase shifting in both the x' and y' directions were processed in the frequency domain to separate the grid moiré projection into double linear moiré fringes in two orthogonal directions. A two-step phase-shifting algorithm was then applied to extract the lateral first-order partial derivative of the phase projection in two orthogonal directions. Furthermore, the radial first-order partial derivative was easily calculated using the double-lateral first-order partial derivative of the phase information. The validation of the proposed phase retrieval method was performed via simulated experiment. The simulated results showed that the theoretical values of the phase information agreed with the phase retrieval results of the

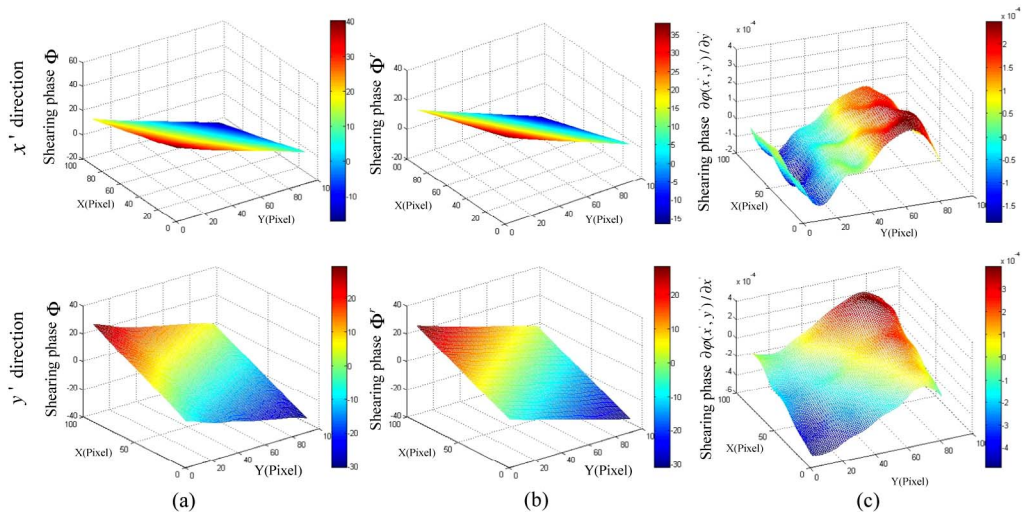

Fig. 13. Extracted shearing phase information: (a) shearing phase information Φ of the deflected interferograms, (b) shearing phase information Φ^r of the reference interferograms, and (c) extracted first-order partial derivatives of the propane flame phase projections $\partial\varphi(x', y')/\partial y'$ and $\partial\varphi(x', y')/\partial x'$ in the x and y directions, respectively.

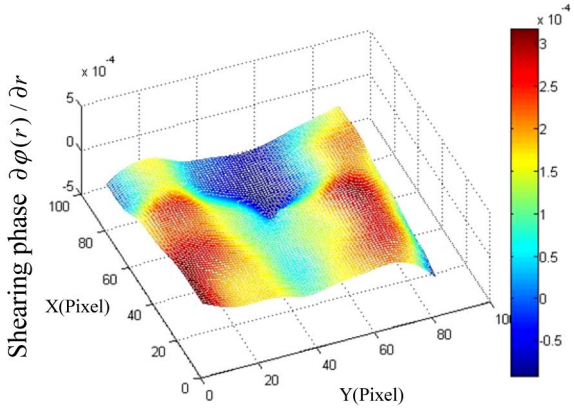

Fig. 14. Extracted first-order partial derivative of the propane flame phase projection $\partial\varphi(r)/\partial r$ in the r direction.

proposed method. Therefore, the proposed phase retrieval method is feasible to measure the radial first-order partial derivative of a phase projection. Finally, the phase retrieval experiment using a propane flame was performed.

The proposed method can be used to measure the radial partial derivative phase information of varied flow fields based on a spatial phase-shifting method by triple-crossed gratings in a compact optical path. This is a basic and important step in MVCT for the reconstruction of a varied flow field's real 3D physical parameters distribution with high accuracy, which will be valuable for monitoring the combustion state in energy engineering and analyzing hypersonic wind tunnel characteristics in aviation and aerospace engineering.

Funding. Natural Science Foundation of Jiangsu Province (BK20150788, BK20170852); Open Research Fund of Jiangsu Key Laboratory of Spectral Imaging & Intelligent Sense (3091601410402, 3091601410411); National Natural Science Foundation of China (NSFC) (61505080, 61701239); Fundamental Research Funds for the Central Universities (30917011320, 30916014112-014).

REFERENCES

1. J. B. Michael, P. Venkateswaran, J. D. Miller, M. N. Slipchenko, J. R. Gord, S. Roy, and T. R. Meyer, "100 kHz thousand-frame burst-mode planar imaging in turbulent flame," Opt. Lett. **39**, 739–742 (2014).
2. X. Cai, J. Liang, Z. Lin, R. Deiterding, and F. Zhuang, "Detonation initiation and propagation in nonuniform supersonic combustible mixtures," Combust. Sci. Technol. **187**, 525–536 (2015).
3. W. Cai and C. F. Kaminski, "A tomographic technique for the simultaneous imaging of temperature, chemical species, and pressure in reactive flows using absorption spectroscopy with frequency-agile lasers," Appl. Phys. Lett. **104**, 034101 (2014).
4. N. Denisova, P. Tretyakov, and A. Tupikin, "Emission tomography in flame diagnostics," Combust. Flame **160**, 577–588 (2013).
5. X. Li and L. Ma, "Volumetric imaging of turbulent reactive flows at kHz based on computed tomography," Opt. Express **22**, 4768–4778 (2014).
6. B. Zhang, Z. Wu, and M. Zhao, "Deflection tomographic reconstructions of a three-dimensional flame structure and temperature distribution of premixed combustion," Appl. Opt. **54**, 1341–1349 (2015).
7. B. Medhi, G. M. Hegde, K. P. J. Reddy, D. Roy, and R. M. Vasu, "Quantitative visualization of high speed flow through optical tomography," in *28th International Symposium on Shock Waves* (University of Manchester, 2011), pp. 3–8.
8. Y. Song, B. Zhang, and A. He, "Algebraic iterative algorithm for deflection tomography and its application to density flow fields in a hypersonic wind tunnel," Appl. Opt. **45**, 8092–8101 (2006).
9. O. Kafri, "Noncoherent method for mapping phase objects," Opt. Lett. **5**, 555–557 (1980).
10. W. Lv, H. Zhou, and J. Zhu, "Implementation of tridirectional large lateral shearing displacement interferometry in temperature measurement of a diffused ethylene flame," Appl. Opt. **50**, 3924–3936 (2011).
11. A. Vouldis, C. Kechribaris, T. Maniatis, K. Nikita, and N. Uzunoglu, "Investigating the enhancement of three-dimensional diffraction tomography by using multiple illumination planes," J. Opt. Soc. Am. A **22**, 1251–1262 (2005).
12. M. Anastasio, Y. Zou, E. Sidky, and X. Pan, "Local cone-beam tomography image reconstruction on chords," J. Opt. Soc. Am. A **24**, 1569–1579 (2007).

13. N. Sun, Y. Song, J. Wang, Z. Li, and A. He, "Volume moiré tomography based on double cross gratings for real three-dimensional flow field diagnosis," Appl. Opt. **51**, 8081–8089 (2012).
14. T. Ramirez-delreal, M. Mora-Gonzalez, F. Casillas-Rodriguez, J. Munoz-Maciel, and M. Paz, "Steps length error detector algorithm in phase-shifting interferometry using Radon transform as a profile measurement," Opt. Express **25**, 7150–7160 (2017).
15. U. Rivera-Ortega, "Phase shifting by wavelength modulation in a cube beam splitter interferometer," Appl. Opt. **56**, 3543–3546 (2017).
16. Y. Wang, X. Qiu, J. Xiong, B. Li, L. Zhong, S. Liu, Y. Zhou, J. Tian, and X. Lu, "General spatial phase-shifting interferometry by optimizing the signal retrieving function," Opt. Express **25**, 7170–7180 (2017).
17. J. E. Millerd and J. C. Wyant, "Simultaneous phase-shifting fizeau interferometer," U.S. patent 7,230,718 (12 June 2007).
18. J. E. Millerd and N. J. Brock, "Methods and apparatus for splitting, imaging and measuring wavefronts in interferometry," U.S. patent 6,304,330 (16 October 2001).
19. N. Toto-Arellano, A. Martinez-Garcia, G. Rodriguez-Zurita, J. Rayas-Alvarez, and A. Montes-Perez, "Slope measurement of a phase object using a polarizing phase-shifting high-frequency Ronchi grating interferometer," Appl. Opt. **49**, 6402–6408 (2010).
20. Y. Song, Y. Chen, J. Wang, N. Sun, and A. He, "Four-step spatial phase-shifting shearing interferometry from moiré configuration by triple gratings," Opt. Lett. **37**, 1922–1924 (2012).
21. Z. Guo, Y. Song, J. Wang, Z. Li, and A. He, "Theoretical analysis and experimental verification of six-step spatial phase-shifting shearing interferometry by double gratings," J. Opt. Soc. Am. A **30**, 1535–1543 (2013).
22. Z. Guo, Y. Song, J. Wang, Z. Li, and A. He, "Two-step spatial phase-shifting lateral shearing interferometry by triple gratings," Opt. Commun. **323**, 110–118 (2014).